

# Steel Beam-Column Connections Using Shape Memory Alloys

Justin Ocel, M.ASCE<sup>1</sup>; Reginald DesRoches, M.ASCE<sup>2</sup>; Roberto T. Leon, M.ASCE<sup>3</sup>;  
W. Gregory Hess<sup>4</sup>; Robert Krumme<sup>5</sup>; Jack R. Hayes<sup>6</sup>; and Steve Sweeney<sup>6</sup>

**Abstract:** This study evaluates the feasibility of a new class of partially restrained connections using shape memory alloys. In the martensitic form, shape memory alloys (SMAs) have the ability to recover large residual deformations by heating the alloy above its transformation temperature. The proposed connection consists of four large diameter NiTi SMA bars connecting the beam flange to the column flange and serve as the primary moment transfer mechanism. Two full-scale connections were tested using the SAC loading protocol. The connections exhibited a high level of energy dissipation, large ductility capacity, and no strength degradation after being subjected to cycles up to 4% drift. Following the initial testing series, the tendons were heated to recover the residual beam tip displacement. After initiating the shape memory effect within the tendons, the connections were retested, displaying repeatable and stable hysteretic behavior. An additional test was performed under dynamic loading to examine the strain rate effects on the performance of the connection. The dynamic tests showed similar behavior, except for a decrease in energy dissipation capacity when compared to the quasi-static tests.

**DOI:** 10.1061/(ASCE)0733-9445(2004)130:5(732)

**CE Database subject headings:** Beam columns; Steel; Connections, semi-rigid; Shape memory effect; Seismic design; Cyclic tests.

## Introduction

In the aftermath of the 1994 Northridge and 1995 Kobe earthquakes, concern has been raised over the unexpected performance of fully restrained welded steel connections. Connections in over 90 welded moment frames in the Northridge area experienced fracture in the welds joining the beam flange to the column due to lack of fusion discontinuities, low toughness weld metal, and the unfused notch left from the back-up bar. Following these earthquakes, the Federal Emergency Management Agency (FEMA) initiated a research effort, known as the SAC Steel Project (FEMA 1995), to investigate deficiencies in current moment connections and evaluate ways of improving connections in steel frames. One of the SAC research initiatives was to evaluate the effectiveness of various types of bolted, partially restrained (PR) connections as an alternative to fully restrained (FR) welded connections (Swanson and Leon 2001).

In the SAC project, bolted connections were found to be a viable alternative to fully welded connections. On the global scale, PR connections have smaller initial stiffnesses and “yielding” strength when compared with fully welded counterparts. Hence more connections are required in lateral bracing systems (Leon 1995), resulting in a tougher and more redundant structural system. On the local scale, properly designed PR bolted connections can provide more yielding mechanisms and alternate load paths than welded connections, resulting in better local ductility when the connection is properly detailed.

However, the performance of PR connections can be improved further by introducing ductile damping connecting elements which will enhance the seismic properties over conventional bolted connections. The aim of this study is to assess the feasibility of SMAs as connecting elements in steel PR connections. Shape memory alloys possess the unique ability to withstand large strain demands (~4–6%) but recover residual strains when heated above their transformation temperature. When SMAs are integrated into a steel connection, they offer the possibility of significantly enhancing the ductility and damping capacity of PR connections. In addition, the unique shape memory behavior provides the possibility of removing the residual deformation within the connection by heating the SMAs above their transformation temperature following a seismic event. In the research reported herein, two proof-of-concept SMA-based connections were tested to determine their cyclic behavior. Following the initial loading protocol, the shape memory effect was initiated by heating the SMAs above their transformation temperature and retested. This paper presents the results from these full-scale connection tests.

<sup>1</sup>PhD Candidate, Univ. of Minnesota, 500 Pillsbury Dr. SE, Minneapolis, MN 55455.

<sup>2</sup>Assistant Professor, Georgia Institute of Technology, Atlanta, GA 30318. E-mail: reginald.desroches@ce.gatech.edu

<sup>3</sup>Professor, Georgia Institute of Technology, Atlanta, GA 30318.

<sup>4</sup>KPFF Consulting Engineers, 1201 Third Ave., Suite 900, Seattle, WA 98101.

<sup>5</sup>Managing Partner, E\*Sorbs Systems, Berkeley, CA 94708.

<sup>6</sup>Seismic & Structural Engineering Group, CERL, U.S. Army Research and Development Center, 2902 Newmark Dr., Champaign, IL 61822-1076.

Note. Associate Editor: Mark D. Bowman. Discussion open until October 1, 2004. Separate discussions must be submitted for individual papers. To extend the closing date by one month, a written request must be filed with the ASCE Managing Editor. The manuscript for this paper was submitted for review and possible publication on July 24, 2002; approved on June 11, 2003. This paper is part of the *Journal of Structural Engineering*, Vol. 130, No. 5, May 1, 2004. ©ASCE, ISSN 0733-9445/2004/5-732-740/\$18.00.

## Shape Memory Alloys

Shape memory alloys are a class of alloys that display several unique characteristics, including Young's modulus-temperature

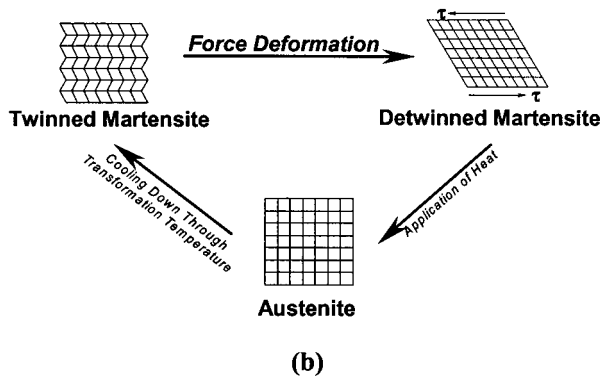
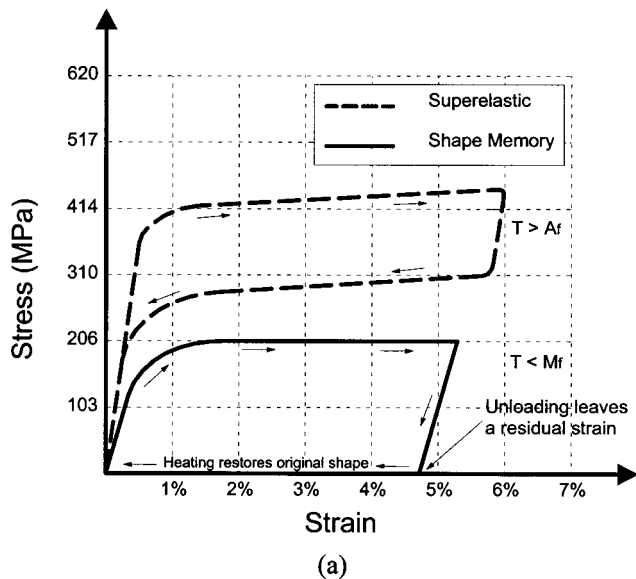


**Fig. 1.** (a) Stress-strain properties of austenitic and martensitic shape memory alloys. Both plots depict one cycle from zero load to a specific strain and back to zero load. (b) Crystallographic changes through shape memory effect.

relations, shape memory effects, pseudoelasticity, and high damping characteristics. During deformation, SMAs will undergo phase transformations instead of intergranular dislocations as typically found in metals. These phase transformations refer to spontaneous shifts between martensitic and austenitic crystal forms. The material properties of the martensite and austenite phases depend upon the temperature and external stress applied to the crystal [see Fig. 1(a)]. At temperatures slightly above  $A_f$  (austenite finish temperature), the material is austenitic. However, the martensitic phase can be stress-induced, resulting in what is commonly referred to as the superelastic, or pseudoelastic, effect. At temperatures below  $M_f$  (martensite finish temperature), the material is in its martensitic form and exhibits the shape memory effect. The crystallographic change during a shape memory effect cycle is illustrated in Fig. 1(b). Fully twinned martensite forms into alternating layers of rhombic shaped crystals (B19' monoclinic structure). After loading the SMA beyond a certain strain threshold, the twinned martensite begins to shift slightly along twin boundaries to accommodate deformation, in what is commonly referred to as the detwinning process. Once the crystal has been detwinned, a residual deformation will remain once the load is removed. However, upon heating the SMA above the  $A_f$  temperature, a phase transformation from martensite to austenite oc-

curs, and any residual deformation is recovered. The austenitic crystal form is a planar arrangement where the atoms align themselves in squares (cubic B2 structure). Upon cooling, the material returns to the twinned martensite form, thus completing the shape memory effect cycle. Shape recovery can either be free or constrained. Free recovery allows the material to recover its original shape completely, whereas constrained recovery can develop large internal forces useful for actuator applications (Baz et al. 1990; Brailovski et al. 1997) or for posttensioning applications (Soroushian et al. 2001).

## Applications of Shape Memory Alloys

In order for SMAs to be viable materials for use in seismic resistant design and retrofit, they need to possess certain characteristics. Some of these characteristics include stable hysteretic behavior, ductility, and large energy dissipation. There have been several studies which have quantified the material properties of shape memory alloys. However, the majority of these studies were related to biomedical applications. Applications including arterial stents (Phatouros et al. 2000), bone plates (Funakubo 1987), and orthodontic wire (Widu et al. 1999) have taken advantage of the shape memory and superelastic properties of shape memory alloys. Since the majority of SMA research has been for biomedical applications, only small and thin cross sections such as wires and ribbons have been investigated. Seismic applications have been implemented using superelastic alloys using wrapped bundles of wires, instead of large bars, due to the uncertainty of size effects when large cross sections are used. One example is the retrofit and rehabilitation of three cathedrals in Italy using wrapped wire superelastic devices (Indirli 2001; Croci 2001). Other applications, only experimentally or analytically researched, include passive damping devices for bridges (Wilde et al. 2000; Delemont 2001) and buildings (Cardone et al. 1999; Inaudi and Kelly 1994; Krumme et al. 1995; Higashino 1996).

## Experimental Program

### Shape Memory Alloy Connection Specifications

Two SMA-based, partial strength, partially restrained moment connections were tested as part of this study. The first connection was designed by the E\*Sorb Systems and the second by researchers at Georgia Tech. The design of the two connections was based on simplifying the analysis of internal forces within the connection and fully exploiting the unique properties of SMAs. This was done through the design of the shear tab which had five holes, one round hole in the center and two slotted holes on either side of the round hole, thus forcing rotation about the center of the shear tab. With rotation forced about the beam's neutral axis, the SMA was fully exploited by placing the tendons on the outside of the beam flanges, maximizing the axial deformation of the tendons. Axial deformations of martensitic SMAs were shown to be the most efficient when compared to bending and torsion deformation modes (MANSIDE 1999). The resulting design did not necessarily reflect that of a typical connection. However, it does allow for a proof-of-concept specimen to address the feasibility of integrating shape memory alloys into steel moment connections.

The first connection tested, S1, joined a W360×237 (W14×159) column to a W610×140 (W24×94) beam using four martensitic Nitinol SMA tendons, two on each flange of the beam, as

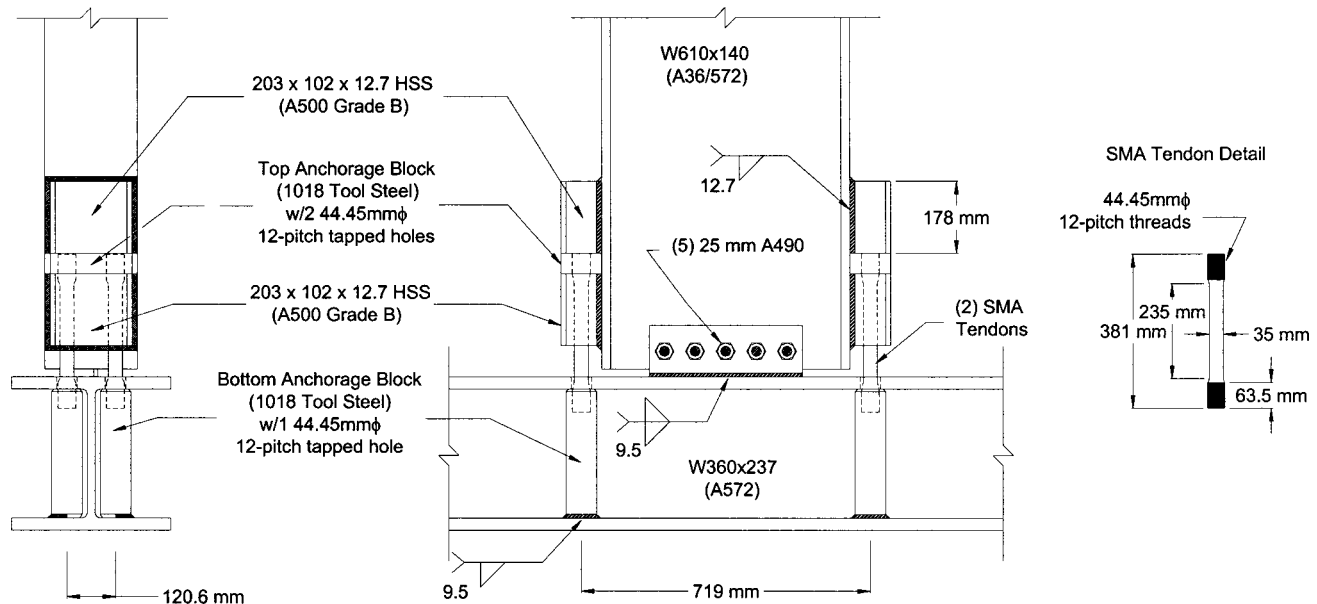


Fig. 2. Details of first shape memory alloy-based connection, S1

shown in Fig. 2. The shear force in the beam was transferred to the column by use of a shear tab, which was 381×127×9.5 mm (15×5×3/8 in.) with five holes for 25.4 mm (1 in.) bolts. The four outer bolt holes of the shear tab had 38.1 mm (1.5 in.) long slots to allow the beam to freely rotate about the standard round hole in the center of the shear tab without the shear tab transferring significant moment to the column. This detail was also intended to enforce rotation about the centroid of the beam, implying equal tension and compression in the tendons. The SMA tendons were 381 mm (15 in.) long with a diameter of 35 mm (1.375 in.) in the 229 mm (9 in.) central gage length. The ends of the tendons were 44 mm (1.75 in.) diameter with a 12-pitch threading; this allowed each tendon to be threaded into two different anchorage blocks. The top anchorage block had dimensions of 50.8×102×203 mm (2×4×8 in.) and was wedged (no mechanical fastening was used) between two 203×102×12.7 mm (4×8×1/2 in.) rectangular tubes using shim stock to fill the gaps between the top anchorage block and rectangular tube. The rectangular tubes were, in turn, fillet welded to the outer beam flange surfaces, allowing the top anchorage block to resist loads in both directions. The bottom anchorage blocks were 76 mm (3 in.) square blocks, long enough to fit in-between the column flanges, and were fillet welded to the column flange opposite of the beam. Since the tendons were rigidly anchored to both the beam and column, they could transfer both tension and compression, and were expected to buckle under compression. Tendon buckling was not constrained in the connections because previous research using martensitic rods with buckling restrained found asymmetric stress-strain and stiffness behavior. The stiffness and strength in compression are higher than in tension (Lui et al. 1998).

The second connection tested, connection S2, utilized the same design philosophy as S1, but the detailing of various elements was slightly altered to address deficiencies found during testing of connection S1. Specifically, the top anchorage block was welded prior to testing and smaller stiffened angles were welded to the top column flange (not shown in Fig. 3) to restrict the out-of-plane movement of the beam flanges, which was encountered in testing of connection S1. This connection used the same column and shear tab but the beam was replaced with a

lighter W610×82 (W24×55) section as shown in Fig. 3, which represented a more realistic connection since the tendons could now develop more of the beam's moment capacity. Two stiffened angles replaced the rectangular tubes used in S1 and were fillet welded to each of the outer flange surfaces of the beam. The top anchorage block was welded between the two stiffened angles instead of relying on friction to keep it in place. The tendons were made from the same martensitic Nitinol composition alloy but the dimensions of the tendons were increased to 457 mm (18 in.) long and 36.5 mm (1.44 in.) diameter in the 273 mm (10.75 in.) gauge length.

### Laboratory Setup

The specimen and load frame utilized for this experiment are shown in Fig. 4. The column was 3,760 mm (148 in.) long, measured from the centerline of the pin supports, and the beam section was 4,534 mm (178.5 in.) from the actuator centerline to the column centerline. A bracing system using a separate load frame with outriggers and angle sections was used to laterally support the beam at three brace points.

The connection was tested using the instrumentation and loading protocols outlined in SAC Report BD-97/02 (SAC 1997). The tests were run in displacement control in accordance with SAC protocol using a closed-loop servovalve hydraulic actuator. The SAC load history is based on the interstory drift angle (rad) which is the actuator displacement divided by the beam length (from actuator centerline to column centerline) using Eq. (1)

$$\theta_{\text{total}} = \frac{\Delta}{L_b} \quad (1)$$

where  $\theta_{\text{total}}$  = total rotation of the connection measured in radians;  $\Delta$  = beam tip deflection (mm); and  $L_b$  = length of beam (4,534 mm). The loading protocol consists of six cycles each of 0.375, 0.5, and 0.75% drift, followed by four cycles of 1% drift, and concludes with two cycles of 1.5, 2, 3, and 4% drift. The fixed displacements were applied to the tip of the beam at a rate of 50.8 mm/min (2 in./min). The total rotation reported is the sum of all rotation components calculated using Eq. (1). The concentrated



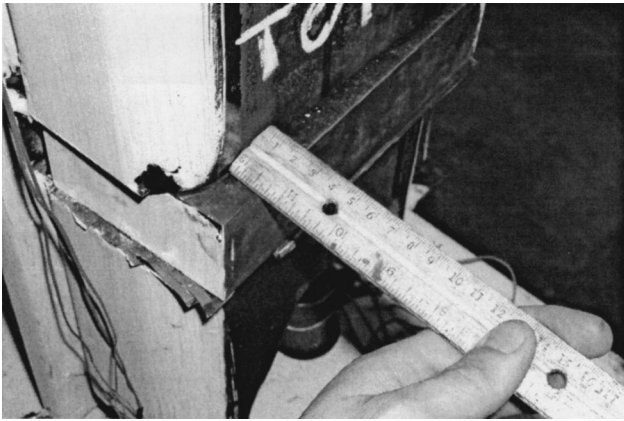


**Fig. 5.** Photo taken at conclusion of initial test of connection S1 depicting top anchorage block movement

dicating it must have been a slow, gradual process. The blocks continued moving throughout the remainder of testing, increasing in amplitude with each load step of the SAC loading protocol. The 3% drift cycles caused severe buckling of the SMA tendons in compression. This cannot be seen in photographs from connection S1 because the tendons were hidden inside the rectangular tubes. However, Fig. 6 shows similar buckling which occurred during testing of connection S2. In the first 4% drift cycle, the buckling of the SMA tendons and lateral translation of the top anchorage block caused a secondary deformation mode that resulted in discontinuation of the test. In this deformation mode, the flanges of the beam began to wrap around the shear tab as a result of a shear force exerted at the top of the tendons from buckling and the misalignment of the tendons from the anchorage block slippage. Since the shear tab was not designed to handle such lateral loads, a 25.4 mm (1 in.) long weld fracture formed on each end of the shear tab after the first 4% drift cycle. For fear of a sudden brittle failure in the shear tab weld, the test was stopped before a second 4% drift cycle could be completed. At the end of the test, connection S1 was left with a residual rotation of 0.005 radians.

As with the S1 connection, specimen S2 behaved elastically through the first three load steps. As with connection S1, there was a small amount of hysteresis in the beginning load steps. The tendons began to scale their oxide coating in the 0.75% drift step.

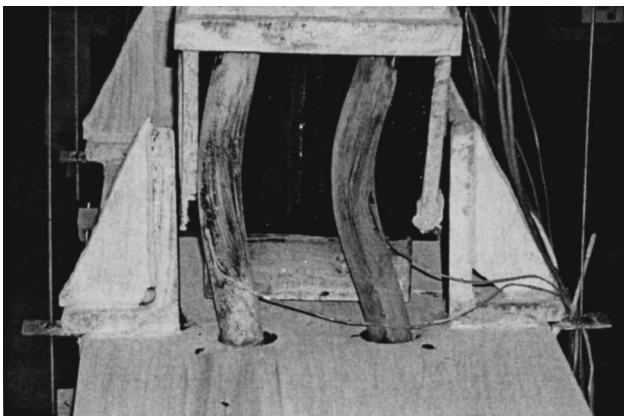


**Fig. 6.** Tendon buckling on connection, S2. Similar buckling was observed in connection S1

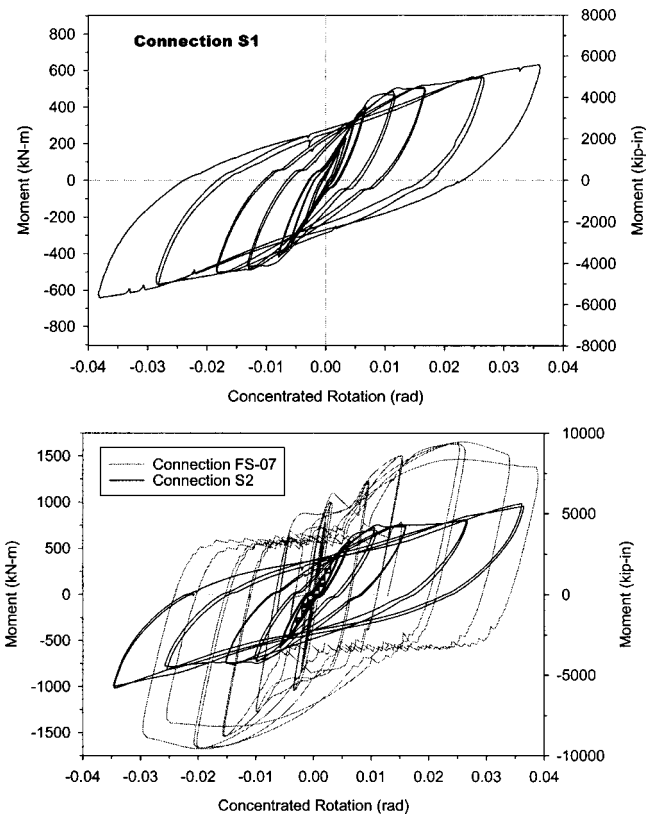


**Fig. 7.** Moment versus concentrated rotation of initial tests for connection S1 (top) and connection S2 plotted with previously tested T-stub connection FS-07 (bottom)

As testing progressed into the 1.5% drift cycles, the beam flanges began to engage against the restraining angles, an indication that the tendons had begun to buckle. This first occurred at the second peak of the first 1.5% drift cycle when the Bottom-South restraining angle became engaged. Once the cycle reversed, the Top-South restraining angle engaged. For the remainder of the test, these beam flanges contacted with the same two restraining angles, as the beam was pushed to drifts exceeding 1.5%. Testing continued until two 4% drift cycles were completed, but was stopped at this stage so proper comparisons could be made to connection S1. At the end of testing, the beam was left with 88.4 mm (3.4 in.) of residual displacement. This residual displacement is quite large when compared to the residual tip displacement of S1. This difference was due to a slight error in the loading protocol for specimen S2. After the last 4% drift peak of connection S2, the tip was not forced to zero displacement and then unloaded to zero force, as in S1. Instead, it was unloaded to zero force immediately, hence not completing the cycle, and leaving a large residual displacement.

The results of the initial testing of both connections yielded similar results. Fig. 7 shows the plots of the moment versus concentrated rotations for the two connections which demonstrate stable hysteresis with no pinching behavior, no strength degradation, and good energy dissipation. In the first 1.5% drift cycle for both connections, there is a perfectly “plastic” part to the hysteresis at the peak of the cycle. This plateau portion signifies that the SMA tendons had begun to detwin. However, the second cycle of 1.5% drift did not show the plateau, indicating that cyclic reversals did not detwin the martensite in the other direction (Xie et al. 1998). This same behavior also occurred in the 2% and 3%

**Table 1.** Connection Property Comparison between Shape Memory Alloy Connections and Previously Tested T-Stub Connections

Specimen	FS-07	FS-08	S1	S2
Beam section <sup>a</sup>	W24×55	W24×55	W24×94	W24×55
Column section <sup>a</sup>	W14×145	W14×145	W14×159	W14×159
Connector <sup>a</sup>	WT10.5×46.5	WT10.5×46.5	1.375φ Tendons	1.4375φ Tendons
$M_{max}/M_p^b$	1.135	1.363	0.447	0.868
Elastic stiffness <sup>c</sup>	2.70E5	2.32E5	7.17E4	7.22E4
kN m/rad (k in./rad)	(2.39E6)	(2.05E6)	(6.35E5)	(6.39E5)
Energy dissipated	5.38E2	5.84E2	4.48E2	5.35E2
kN m (k in.) <sup>d</sup>	(4.76E3)	(5.17E3)	(3.97E3)	(4.74E3)

<sup>a</sup>Section sizes are in English units.

<sup>b</sup> $M_p$  is based on  $\phi=1.0$  and  $F_y$  from mill certificates.

<sup>c</sup>Represents the initial stiffnesses (secant stiffness at 0.375% drift).

<sup>d</sup>Dissipated energy is recorded as the integration of the moment versus total rotation hysteresis up until connection failure.

cycles, but did not occur in the 4% drift cycle, meaning the SMA tendons had exhausted their stress plateau and begun to strain harden.

Both connections were cycled to maximum drifts of 4%. However, Fig. 7 shows the maximum concentrated rotations between 3.5% and 3.8% corresponding to 4% total rotation. Summing all components of rotation, the concentrated rotation is approximately 80–95% of the total rotation after accounting for elastic beam and column deformation, and panel zone shearing. Since no inelasticity occurred in the steel elements, the SMA tendons are responsible for this concentrated rotation.

Table 1 compares the two SMA connections tested against two previously tested T-stub connections at Georgia Tech (Smallidge 1999). As shown in Table 1, the elastic stiffnesses for the T-stub connections are considerably larger than that for the SMA connection. This difference in stiffness is primarily due to the low value of the modulus of elasticity for NiTi SMA compared with structural steel. The modulus of elasticity for martensitic NiTi SMA is typically on the order of 21–41 GPa, compared with approximately 200 GPa for steel. This is clearly an issue that would need to be addressed when considering the use of this type of connection. Table 1 also shows a comparison of the total energy dissipated between the T-stub and SMA connections. Although the energy dissipated per cycle is clearly less in the SMA connection (as shown in Fig. 7, bottom), the total energy is approximately the same, since the SMA connection was subjected to more loading cycles before failing.

### Initiating Shape Memory Effect

After each connection was initially tested, the tendons were heated above their transformation temperature to initiate the shape memory effect and attempt to recover the residual tip displacement in the beam. Two different methods were used to heat the tendons above their  $A_f$  temperature of approximately 93°C (200°F). Since a significant amount of heat was required, propane torches were found to be most effective for connection S1. As the tendons were being heated with the torches, the actuator applied a 22 kN (5 kip) force in a direction to help the tendons recover their shape. After eight minutes, the propane torches heated the tendons to 288°C (550°F), bringing the total recovered displacement to 18 mm (0.7 in.), which corresponds to a 76% recovery of residual tip displacement.

During the recovery phase for S2, the ability to initiate the shape memory effect was investigated while the connection was under load, simulating dead load moments expected in a typical connection. The shape memory process is both thermal and mechanical, meaning that an increase in stress is equivalent to a decrease in temperature. Therefore, placing a stress on the tendons (via the imposed load) should result in a requirement for a higher temperature to initiate the shape memory effect. The constant load was created by putting the actuator into load control with –44.5 kN (–10 kip) force at the beam tip in a direction resisting the motion of the beam during the straightening process. This load corresponds to approximately 138 MPa (20 ksi) of stress in each tendon. Each side of the connection was heated simultaneously with two torches, one on each tendon. The first heating cycle lasted for 15 min and recovered 20 mm (0.787 in.) of tip displacement. This corresponded to an approximate recovery of 20% of the residual displacement. Since these results were less than desirable, it was decided to change the load in the actuator to +2.2 kN (+0.5 kip) to help tendons recover their shape, and heating continued for an additional 12 min, which recovered another 19.5 mm (0.768 in.). In total, 39.5 mm (1.555 in.) of tip displacement was recovered, which is only 39.5% of the total. At this point, the surface temperature of one tendon was measured with a thermocouple to be ~254°C (490°F). The propane torches still were not achieving the desired results and it was determined that more heat needed to be applied to the tendons. An oxy-acetylene torch with a no. 8 rosebud was used to heat the tendons of S2 a second time. The actuator was kept in load control with +3.6 kN (+0.8 kip) of load applied at the beam tip, again to help the tendons recover their shape. The oxy-acetylene torch was able to get the tendon surface temperature up to 400°C (752°F), measured with a thermocouple. Through 27 min of heating, only another 13 mm (0.499 in.) of beam tip displacement was recovered, resulting in a total beam tip recovery of 41.4 mm (2.054 in.) through the two heating iterations, which corresponds to 54.1% total recovery. Fig. 8 shows how much shape recovery actually occurred within the tendons themselves, with dotted lines showing the residual shape superimposed with the actual picture taken after the heat straightening process.

### Retesting Connections

Once the tendons were straightened, the connection was subjected to a modified version of the SAC protocol to address the cyclic

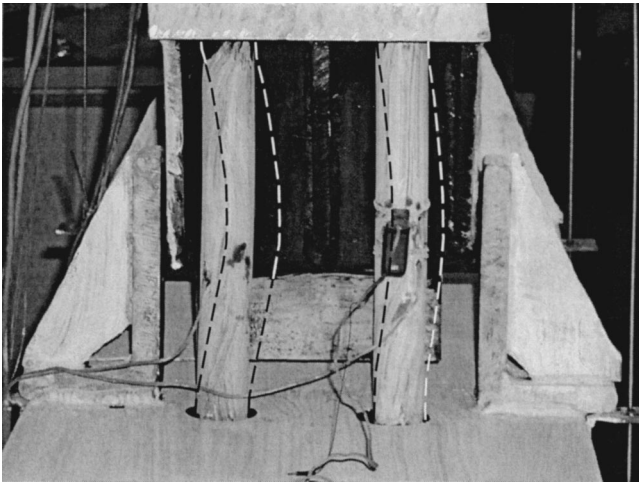


**Fig. 8.** Photo of connection S2 tendons after heating; dashed lines represent residual shape before heating

stability of the connections at high drifts. The modified protocol consisted of 1 cycle of 0.5, 0.75, 1, 1.5, 2, and 3% drift, followed by 20 cycles of 4% drift. Before S1 could be retested a thicker weld was placed over the old shear tab weld to address the fracture in the weld toe. In addition, the top anchorage block was fully welded to fix any translational degrees of freedom. Finally, small angle sections were welded to the column flange to prevent out-of-plane distortions of the beam flanges. Connection S2 did not need any modifications because its original design addressed the issues of out-of plane beam flange distortions.

Connection S1 made it through the eighth 4% drift cycle before one of the tension tendons fractured near the peak of the cycle. Loading was continued until the second tension tendon fractured, at which point the connection was considered to have failed. Both of the tendons that broke in connection S1 fractured at the transition radius from the gauge length to the threaded end of the tendons. Connection S2 made it through the modified protocol up to the eighth 4% drift cycle when loading ceased.

Fig. 9 shows the moment versus concentrated rotation for the retest of both connections after the tendons had been heat straightened. The hysteresis loops for connection S2 showed an asymmetry during cycling. This was probably due to the fact that after heat straightening, the buckled tendons never completely straightened out. Since the tendons were prebuckled before the retest began, the small drift cycles did not induce enough beam tip displacement to cause the prebuckled tendons to straighten out. However, after the first 4% drift cycle, the connection began to show a symmetric behavior.

Several comments can be made regarding the retesting of the connections. First, the moment-rotation behavior in the retest is nearly identical to that observed during the initial test. This is best shown in Fig. 10, which superimposes the first 4% drift cycle for the initial and retest of connection S1. Results from connection S2 are similar. Second, the hysteresis loops for the eight consecutive 4% drift cycles demonstrate repeatability with no stiffness degradation for both of the connections, whereas conventional connections most likely would demonstrate some stiffness degradation at this displacement level. The stable hysteretic behavior is a direct result of the stable cyclic behavior in the shape memory alloys. Individual tests of the SMA components used in the connection showed a repeatable stable hysteresis with no stiffness or strength degradation for strains <4% and an increase in strength for

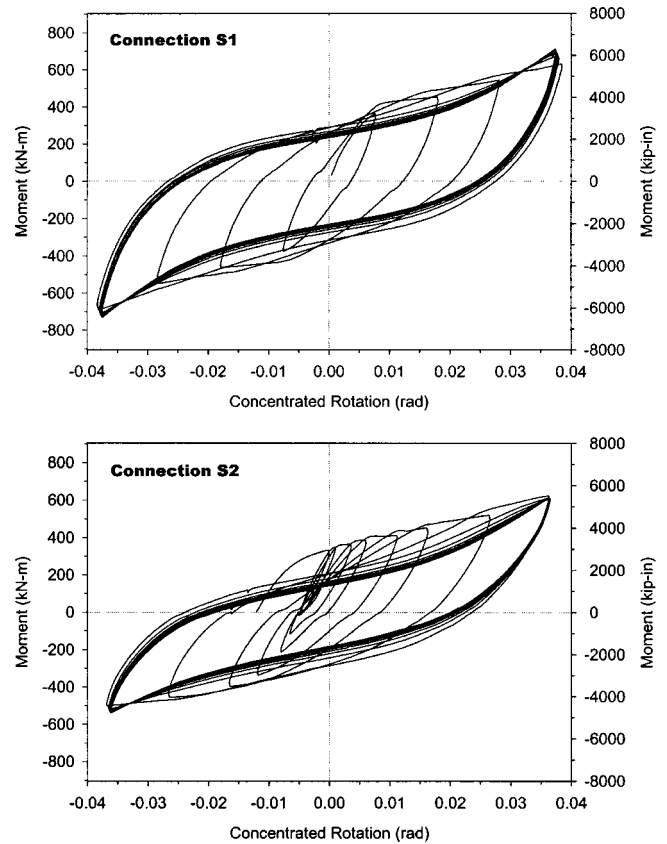


**Fig. 9.** Moment versus concentrated rotation of retest for connection S1 (top) and connection S2 (bottom)

strains beyond 4% (Ocel 2002). Previous researchers have shown similar behavior (Lui et al. 1999). Since the SMA tendons are the load transfer mechanism in the connection, this behavior can be directly extrapolated into the moment/rotation behavior of the connection. Finally, the hysteresis loops of the retest show a plateau at the first peaks of moderate drift intensities, signifying detwinning of the SMA tendons was occurring. This indicates that the shape memory effect was at least partially initiated during the heat straightening process even though the recovery of residual beam tip displacement was not complete.

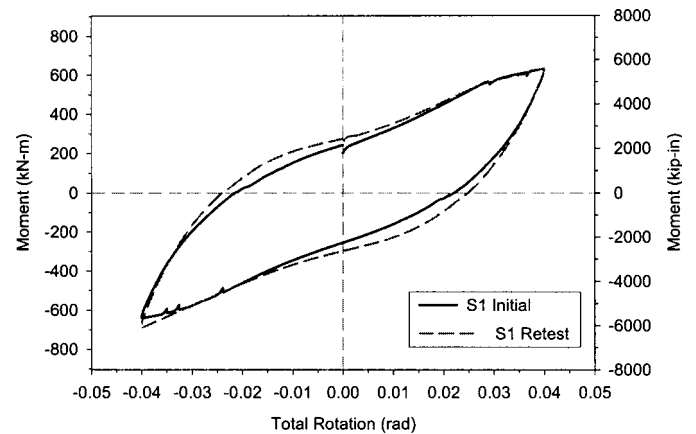


**Fig. 10.** Hysteresis comparisons of initial and retests of connection S1; data are similar for connection S2

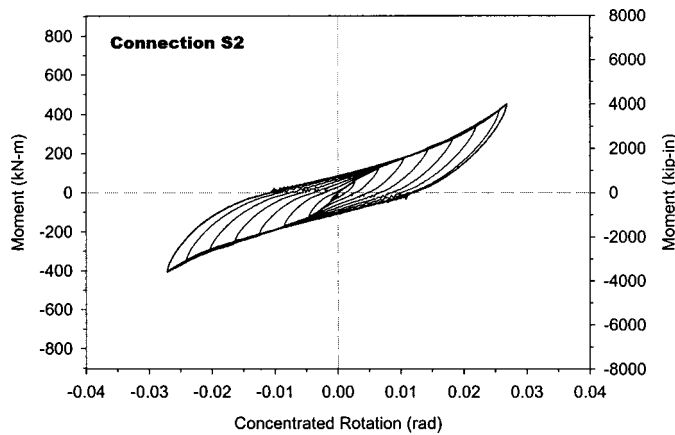


**Fig. 11.** Moment versus concentrated rotation for connection S2 dynamic test (3% drift cycle at 0.25 Hz)

### Dynamic Testing of Connection S2

Several studies on the strain rate effects in martensitic shape memory alloys have been performed. Liu et al. (1999) found that the damping properties were insensitive to strain rate for samples tested at 0.01 Hz to 0.5 Hz at a maximum strain of 4%. However, for higher strain rates, studies have shown that there is a decrease in energy dissipation in the martensitic SMAs (Ocel 2002; MAN-SIDE 1999). Since previous studies have led to conflicting information, connection S2 was tested for a third time with large beam tip displacement rates (henceforth referred to as dynamic loading).

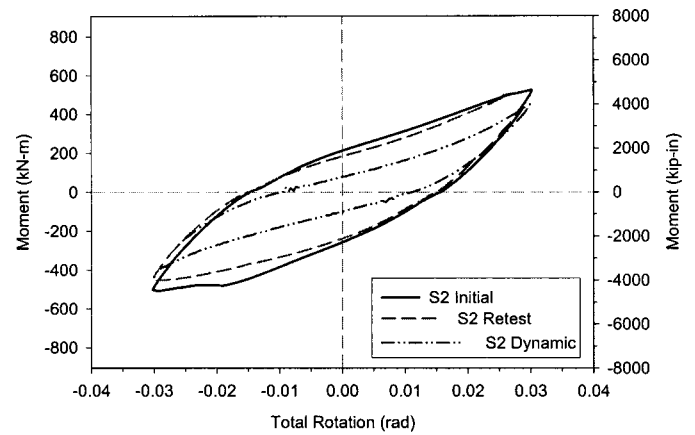
The first dynamic loading consisted of 15 cycles at 3% drift, using a sine wave function at a frequency of 0.15 Hz, and was primarily performed to gauge the response of the actuator. After this first dynamic loading, slight adjustments were made to the data acquisition and hydraulic systems before a second loading was induced. The second dynamic loading continued with 3% drift cycles at 0.25 Hz. This loading rate would induce  $\pm 3.95\%$  strain cycles in the SMA tendons at a rate of 1% strain/s. After five cycles, the Top-North (see Fig. 4) tendon fractured within the top anchorage block, indicating failure of the connection.

Fig. 11 shows a graph of the moment versus concentrated rotation through the dynamic test just before the SMA tendon fractured. The outer loop shows five 3% drift cycles together, with identical behavior, thus confirming the repeatable performance of the SMA connection. The most obvious feature of the dynamic hysteresis is the pronounced difference in energy dissipation between the initial and retests. The energy dissipated during the dynamic test is approximately 1/3 that of the initial test, signifying that the martensitic tendons display obvious strain rate effects. This is also clearly shown in Fig. 12, which shows a comparison of the first 3% moment versus concentrated rotation cycle for the initial, retest, and dynamic tests for connection S2.

### Conclusions

This study investigated the effectiveness of partially restrained connections using shape memory alloy connecting elements. This proof-of-concept study resulted in the following conclusions:

1. SMA connections exhibited stable hysteresis, with no strength degradation in their initial testing up to the 4% drift level. The martensitic SMA tendons were used as a moment



**Fig. 12.** Moment versus total rotation comparisons for connection S2

resistance connection element, but doubled as a deformation fuse. SMAs have very high deformation capacity, so at high connection rotations the energy can be dissipated through the SMA tendons and not through yielding mechanisms in the beams and columns. The concept of a deformation fuse was confirmed with these tests as no significant yielding was observed in the beam and column sections.

2. After the connections were tested, the tendons were heated to initiate the shape memory effect. The recovery of residual displacement was attempted with load (simulated dead load moment) and no load. Both connections failed to completely recover the original shape of the tendons under load. However, without load, the tendons were able to recover 76% of the beam tip displacement when unconstrained and 54% when load constrained.
3. Once the shape memory effect was initiated and the tendons were straightened, both were retested. Each connection showed nearly identical hysteretic behavior during the retest to that in the initial test for both connections S1 and S2. In the retest, the loading protocol specified each connection be subjected to eight 4% drift cycles. The hysteresis loops of the eight 4% drift cycles were identical, with no loss in strength, stiffness, or any signs of fatigue. This implies these hybrid connections could be reused following a seismic event, if the tendons can be appropriately heated to initiate the shape memory effect.
4. The results of this proof-of-concept test show promise for the use of shape memory alloys in seismic resistant design and retrofit. However, several factors would need to be considered, including the cost of the material and the methodology used for the connection of the SMA component to the structure. The cost of shape memory alloys has decreased significantly in the past few years from over \$1,110/kg in 1996 to less than \$111/kg today. It is expected that as more commercial applications use SMAs in large quantities, the cost will continue to decrease. However, a potentially more challenging issue is how these materials will be connected to the structure under consideration. Welding has proven difficult, since it creates a brittle region around the welding zone, and machining is difficult and expensive.

### Recommendations for Future Work

The two connections tested were designed to evaluate the efficacy of shape memory alloys in steel beam-column connections. The

results from this proof-of-concept test proved very promising. However, a few areas still need further research:

1. More field applicable connections need to be designed. The two connections placed the tendons on the outside of the beam flanges to maximize the strain in the tendons. However, this can possibly interfere with composite slab systems. Other types of connections should either place the tendons level with the beam flanges, or under the beam flange next to the web.
2. Initiating the shape memory effect in large diameter martensitic SMA tendons needs more investigation. The tendons used in this study were not able to completely restore the connections to their original geometry, partly due to the difficulty in providing uniform and adequate heat to such a large section. One way to alleviate this problem would be to use many small diameter bars in parallel to equate the strength of a large diameter tendon. In addition, the effect of stress on the ability to initiate the shape memory effect needs further study.
3. Analytical studies need to be performed to evaluate the effectiveness of the SMA connection in improving the seismic performance of the building. Using a fiber model of the connection, the effects of tendon length, diameter, type of SMA (martensitic or austenitic), number of tendons, and overall connection geometry can be evaluated.

## Acknowledgments

This work was supported primarily through a joint effort of E\*Sorbs Systems and the Construction Engineering Research Laboratory (CERL), U.S. Army Engineering Research and Development Center. Additional funding was provided by the Earthquake Engineering Research Centers Program of the National Science Foundation under Grant No. EEC-9701785 (Mid-America Earthquake Center), and the CAREER program of the National Science Foundation under Grant No. 0093868.

## References

- Baz, A., Imam, K., and McCoy, J. (1990). "Active vibration control of flexible beams using shape memory actuators." *J. Sound Vib.*, 140, 437–456.
- Brailovski, V., Trochu, F., and Leboeuf, A. (1997). "Design of shape memory linear actuators." *Proc. SMTS Conf.*, Asilomar, Calif.
- Cardone, D., Dolce, M., and Marnetto, R. (1999). "Devices based on nickel-titanium alloys for the seismic protection of civil structures." *SMST-99 Proc., 1st European Conf. on Shape Memory and Superelastic Technologies*, Antwerp Zoo, Belgium.
- Croci, G. (2001). "Strengthening of the basilica of St. Francis of Assisi after the September 1997 Earthquake." *Structural Engineering Int.*
- Delemont, M. (2001). "Seismic retrofit of bridges using shape memory alloys." MS thesis, School of Civil and Environmental Engineering, Georgia Institute of Technology, Atlanta.
- FEMA. (1995). "Steel moment frame structures: Background reports." *FEMA-288*, Federal Emergency Management Agency.
- Funakubo. (1987). *Shape memory alloys*, Gordon and Breach, New York.
- Higashino, M. (1996). "Experimental and analytical studies of structural control system using shape memory alloy." *2nd Int. Workshop on Structural Control*, 221–232.
- Inaudi, J., and Kelly, J. (1994). "Experiments on tuned mass dampers using viscoelastic, frictional and shape memory alloy materials." *Proc., 1st World Conference on Structural Control*, 127–136.
- Indirli, M., Castellano, M., Clemente, P., and Martelli, A. (2001). "Demo-application of shape memory alloy devices: The rehabilitation of the S. Giorgio Church bell tower." *Proc. SPIE, Smart Structures and Materials*.
- Krumme, R., Hayes, J., and Sweeney, S. (1995). "Structural damping with shape memory alloys: One class of devices." *Proc. SPIE (The International Society for Optical Engineering), Smart Structures and Materials Conf.*, Paper No. 2445-21, San Diego.
- Leon, R. T. (1995). "Seismic performance of bolted and riveted connections." *FEMA-288, Background Reports: Metallurgy, Fracture Mechanics, Welding, Moment Connections and Frame Systems Behavior*.
- Lui, Y., Li, Y., Ramesh, K. T., and Van Humbeeck, J. (1999). "High strain rate deformation of martensitic NiTi shape memory alloy." *Scr. Metall.*, 41(1), 89–95.
- Lui, Y., Xie, Z., Van Humbeeck, J., and Delaey, L. (1998). "Asymmetry of stress-strain curves under tension and compression for NiTi shape memory alloys." *Acta Metall.*, 46(12), 4325–4338.
- Lui, Y., Xie, Z., Van Humbeeck, J., and Delaey, L. (1999). "Cyclic deformation of NiTi shape memory alloys." *Mater. Sci. Eng., A*, 273–275, 673–678.
- MANSIDE (1999). "Memory alloys for new seismic isolation and energy dissipation devices." *Proc. MANSIDE Project, Rome*, 1999, 28–29.
- Ocel, J. M. (2002). "Cyclic behavior of steel beam-column connections with shape memory alloy connecting elements." MS Thesis, School of Civil and Environmental Engineering, Georgia Institute of Technology, Atlanta.
- Phatouros, C. C., et al. (2000). "Endovascular stenting for carotid artery stenosis: Preliminary experience using the SMA recoverable technology (SMART) stent." *Am. J. Neuroradiol.*, 21(4), 732–738.
- SAC (1997). "Protocol for fabrication, inspection, testing and documentation of beam-column connection test and other experimental specimens." *SAC Rep. SAC/BD-97/02*, SAC Joint Venture, Sacramento, Calif.
- Smallidge, J. M. (1999). "Behavior of bolted beam-to-column T-stub connections under cyclic loading." thesis presented to School of Civil and Environmental Engineering, Georgia Institute of Technology, Atlanta.
- Soroushian, P., Ostowari, K., Nossoni, A., Chowdury, H. (2001). "Repair and strengthening of concrete structures through application of corrective post-tensioning forces with shape memory alloys." *Transportation Research Record 1770*, Transportation Research Board, Washington, D. C., 20–26.
- Swanson, J., and Leon, R. (2001). "Stiffness modeling of bolted T-stub connection components." *J. Struct. Eng.*, 127(5), 498–505.
- Widu, F., Drescher, D., Junker, R., and Bourauel, C. (1999). "Corrosion and biocompatibility of orthodontic wires." *J. Mater. Sci.: Mater. Med.*, 10(5), 275–281.
- Wilde, K., Gardoni, P., and Fujino, Y. (2000). "Base isolation system with shape memory alloy device for elevated highway bridges." *Eng. Struct.*, 22, 222–229.
- Xie, Z., Liu, Y., and Van Humbeeck, J. (1998). "Microstructure of NiTi shape memory alloy due to tension-compression cyclic deformation." *Acta Mater.*, 46(6), 1989–2000.